Performance Analysis and Design Considerations of the Near-Field-Focused Rotman Lens Antennas

Salem M. Otman, Mehmet Kuşaf, and Abdullah Y. Öztoprak

Department of Electrical and Electronic Engineering
Cyprus International University, Nicosia 99258, Northern Cyprus
22007405@student.ciu.edu.tr, mkusaf@ciu.edu.tr, aoztoprak@ciu.edu.tr

Abstract – This study investigates the application of Rotman lens antennas in the near field. The design equations of these antennas have been derived in the near field and demonstrated to be highly effective. By considering specific examples, the shapes of the inner surfaces of these lens antennas have been analyzed and discussed, revealing how practically realizable lens surfaces can be designed. As these Rotman lenses are perfect at only three points in the near field, they exhibit phase errors at other points along a line connecting the three near-field focal points, resulting in deterioration of the near-field patterns. It has been shown that by selecting the lens parameters appropriately, these phase errors can be kept to a minimum, causing only minimal beam deterioration. Compared to far-field-focused Rotman lens antennas, near-field-focused Rotman lens antennas achieve significantly higher power levels, having 3.8 to 6.3 dB improvement for different beams of a 17-element array. The study has demonstrated the potential of Rotman lenses as multiple beamforming antennas for near-field applications.

Index Terms – Beamforming, near-field-focusing, Rotman lenses.

I. INTRODUCTION

Near-field-focused antennas have been extensively used for applications requiring high concentrations of electromagnetic fields in the nearby regions of the antennas [1–9] some applications such as radio frequency identification (RFID) [10–12] and industrial inspection systems [13]. In the case of hyperthermia applications [4, 14–16], concentrating the power on the unhealthy tissues avoids heating and damaging healthy tissues.

On the other hand, only a limited region can be covered with a single focused beam. To increase the coverage area the focused beam should be scanned or multi-beam antenna techniques should be used. Although beam scanning and multiple beamforming is well known and widely published for far-field-focused beams [17–25], there has been a limited number of publications for near-field-focused beams. In [22] the near-field-focused beam is scanned by changing the frequency by introducing progressively increasing multiple additional transmission lines into the system. In [26] the authors compare an electronic scanning antenna using phase shifters and power dividers, with multiple beamforming antennas using Butler matrix and Rotman lens for near-field-focused fields. Butler matrixes are well established beam forming networks using phase shifters and power dividers [27], feeding linear array antennas. Rotman lens beamforming antennas are two dimensional multi-focal constrained lens antennas using a parallel plate region, with several input and output ports, and different lengths of transmission lines.

In this paper we establish the design equations of the Rotman lens beamforming antenna when focusing at three points in the near field instead of three far-field directions. The shape and feasibility of the lens curves have been investigated for different lens parameters. The near-field performance of the near-field-focused lens has been studied for different parameters and compared with the far-field-focused lens.

II. LENS DESIGN

The mathematical model of the near-field-focused Rotman lens is given in Fig. 1. The two-dimensional coordinate system (x,y) centered at O_1 and the coordinate system (X,Y) centered at O_2 are independent of each other. The feed array curve and the inner array curve are represented by the coordinate system centered at O_1 and the radiating array and the target points are represented by the coordinate system centered at O_2. In this study, all lengths are expressed in terms of wavelengths to have frequency independent equations.

The Rotman lens is a two-dimensional lens characterized by constrained paths, or transmission lines, connecting its two surfaces. These surfaces are represented by two curves - the inner lens curve and the outer lens curve - which forms the radiating array. In this study, a linear radiating array is employed, but curved arrays can also be utilized. The Rotman lens's focal points are located at F_1, F_0, and F_2 along the feed array curve, where all feed antenna elements are situated. Points B_1,

Submitted On: December 15, 2023
Accepted On: August 27, 2024

https://doi.org/10.13052/2024.ACES.J.390601

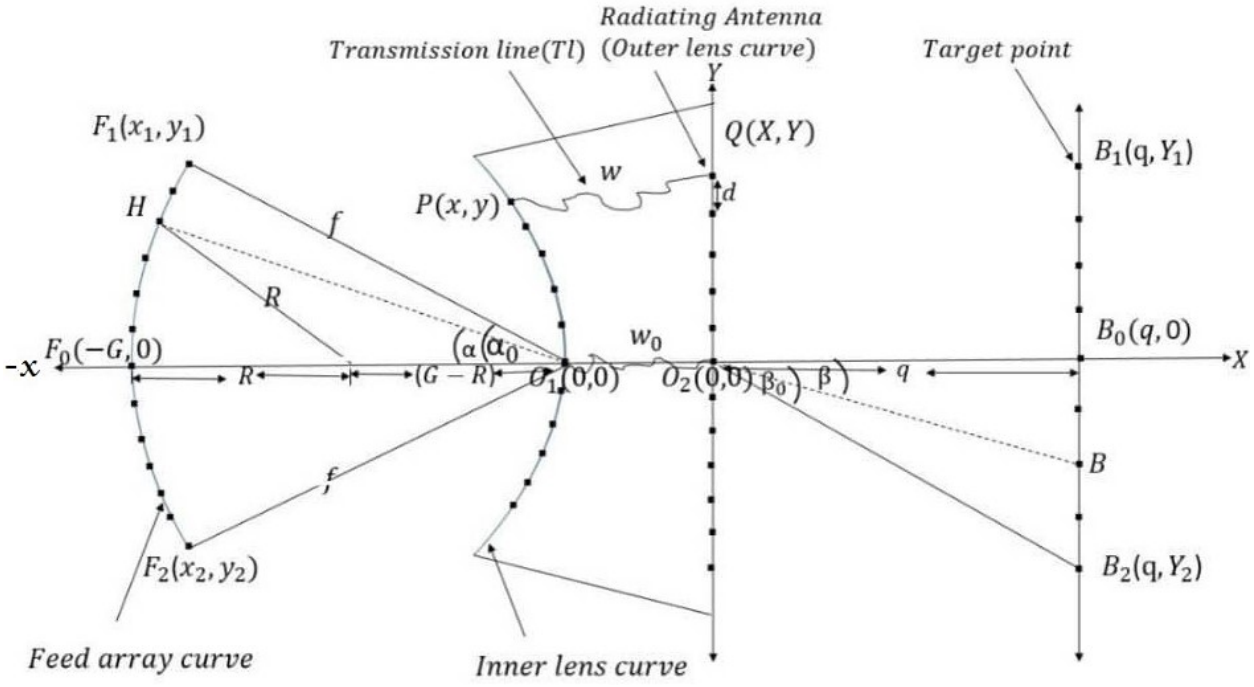

Fig. 1. Geometry of near-field-focused Rotman lens.

B_0, and B_2 in the radiating array's near field represent the locations where the antenna elements at the three lens focal points focus their fields. Element F_1 focuses at B_2, element F_0 focuses at B_0, and element F_2 focuses at B_1. G is the distance from O_1 to the central focal point at F_0.

A general point on the lens's inner curve is denoted by $P(x,y)$, and its corresponding point on the radiating array is represented by $Q(X,Y)$. An antenna element at P receives the field from the feed array elements and relays it to the corresponding element Q at the radiating array via a transmission line of length w .

For a field launched at focal point F_1 to focus at B_2:

$$\left(\vec{F_1P}\right)+w+\left(\vec{QB_2}\right)=(\vec{F_1O_1})+w_0+\left(\vec{O_2B_2}\right). \quad (1)$$

For a field launched at focal point F_2 to focus at B_1:

$$(\vec{F_2P})+w+\left(\vec{QB_1}\right)=(\vec{F_2O_1})+w_0+\left(\vec{O_2B_1}\right). \quad (2)$$

For a field launched at focal point F_0 to focus at B_0 :

$$\left(\vec{F_0P}\right)+w+\left(\vec{QB_0}\right)=G+w_0+\left(\vec{O_2B_0}\right), \quad (3)$$

where w_0 is the transmission line length for the center element.

$$\left(\vec{F_1P}\right)=\sqrt{(x-x_1)^2+(y-y_1)^2}, \quad (4)$$

$$\left(\overline{F_2P}\right)=\sqrt{(x-y_2)^2+(y-y_2)^2}, \quad (5)$$

$$\left(\overline{F_0P}\right)=\sqrt{(x+G)^2+y^2}, \quad (6)$$

$$\left(\overline{QB_2}\right)=\sqrt{(q-X)^2+(Y_2-Y)^2}, \quad (7)$$

$$\left(\overline{O_2B_2}\right)=\sqrt{(q)^2+(Y_2)^2}, \quad (8)$$

$$\left(\overline{QB_1}\right)=\sqrt{(q-X)^2+(Y_1-Y)^2}, \quad (9)$$

$$\left(\overline{O_2B_1}\right)=\sqrt{(q)^2+(Y_1)^2}, \quad (10)$$

$$\left(\overline{QB_0}\right)=\sqrt{(q-X)^2+(Y)^2}, \quad (11)$$

$$\left(\overline{O_2B_0}\right)=\sqrt{(q)^2}, \quad (12)$$

where $x_1 = x_2 = -f\cos\alpha_0$, $y_1 = f\cos\alpha_0$, $y_2 = -f\cos\alpha_0$. Here, f is the distance from O_1 to the off-center focal point at F_1, and α_0 is the angle subtended by off axis lens focal points from O_1.

Equations 1, 2, and 3 are solved simultaneously to determine the variables x, y, and w for each position of Q on the radiating array. The Q positions correspond to the locations of the radiating array antenna elements. The values of x and y define the inner lens curve of the lens, and each point on the inner curve is associated with a corresponding value of w.

In practice the region between feed array and inner lens is a parallel plate region and a TEM wave propagates in this region. The Rotman lenses are usually implemented on microstrip substrates for low power applications and air-filled parallel conducting plates for high power applications. The varying length transmission lines between the inner lens curve elements and radiating elements are usually microstrip lines for the microstrip implementation and co-axial transmission lines for the conducting plate implementation. Usually small V- shaped or stepped transitions [28] are used between the transmission lines and parallel plate region. The transitions act as two-dimensional aperture antennas into the parallel plate region. The field at the target point is obtained by summing the fields of each element at this point.

III. SHAPE OF THE INNER LENS CURVES

The lens design principles outlined above utilize optical principles to generate inner lens curves. Not all inner lens curves obtained in this manner are suitable for practical applications. Given that Rotman lenses operate at microwave frequencies, the shape of the inner lens curves must facilitate efficient power transfer between antenna elements on the feed array curve and those on the inner lens curve. Sample inner lens curves are presented in this section to illustrate the significance of their shapes.

The positions of the lens focal points F_1, F_2, and F_0, the focusing points in the near field B_1, B_2, and B_0, and the length of the radiating array are parameters selected in advance according to the specific application requirements. The parameters for this lens shape study are as follows: the lens focal points are located at $F_1(x_1, y_1)$, $F_2(x_2, y_2)$, and $F_0(-G, 0)$. F_1 and F_2 subtend an angle of 25° (α_0) degrees from the origin O_1. The linear radiating array comprises 17 elements with a separation (d) of 0.5 between them.

The three focusing points in the near field are positioned on a line perpendicular to the $X-$axis and passing through $B_0(q, 0)$. The near-field-focusing points are located at $B_1(q, Y_1)$, $B_0(q, 0)$, and $B_2(q, Y_2)$, where $q = 10$ and $Y_1 = -Y_2 = q * \tan(\beta_o)$. The angle of the off-axis near-field-focusing point is defined as β_o. Here, β_0 is chosen to be 35°. All lens parameters were selected such that the lens is symmetric around the x-axis.

Examples of the inner lens curves, obtained through numerical solutions to equations 1, 2, and 3, have been generated for different values of g, where $g = G/f$. Table 1 shows the G, g, and f values used to obtain the inner lens curves. Figure 2 depicts the shapes of the inner curves for $g = 1.0, 1.05, 1.10, 1.15, 1.20, 1.25, 1.30$, and 1.35 respectively.

The shape of the inner lens curve significantly impacts the illumination of antenna elements and the overall effectiveness of the lens antenna. As shown in Fig. 2 (g=1.35), the inner lens curve bends backward at both the upper and lower end points. This positioning blocks any antenna elements at these locations by those placed before them. Consequently, the antenna elements at the upper end of the inner curve receive very low illumination from the lower end feed elements, and the elements at the lower end of the inner curve receive incomplete illumination from the upper end feed elements.

Table 1: Parameters of the lens design

G	g	f
10.5	1.00	10.5
10.5	1.05	9.52
10.5	1.10	9.09
10.5	1.15	8.69
10.5	1.20	8.33
10.5	1.25	8.00
10.5	1.30	7.69
10.5	1.35	6.66

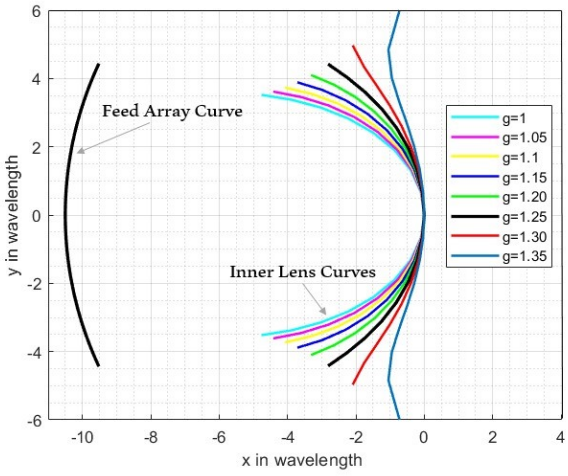

Fig. 2. Lens curves for g=1, 1.05, ..., 1.35.

Conversely, in Fig. 2 (g=1.0), the end elements of the inner curve are bent forward, so the inner curve's lower endpoints will not be illuminated by the lower elements of the feed array curve. Similarly, the inner curve's upper elements will not be illuminated by the upper elements of the feed array curve.

In contrast, Fig. 2 (g=1.25) demonstrates a design where the antenna elements on the feed array curve and inner curve directly face each other without any blockage. This alignment ensures efficient power transfer and maximizes the lens antenna's performance.

The lens antenna shapes presented in Fig. 2 highlight the criticality of selecting appropriate lens parameters for optimal design. Factors such as the positions of the near-field-focusing points and the spacing between radiating array elements can significantly alter the shape of the inner lens curve. Therefore, careful selection of lens parameters is essential for each design to achieve practical realization of these lens antennas.

In summary, the shape of the inner lens curve and the selection of appropriate lens parameters are crucial aspects in designing efficient and high-performance lens antennas. Careful consideration of these factors can optimize power transfer and minimize blockage, leading to enhanced lens antenna performance.

Achieving the strongest possible near-field intensity with a given amount of power requires careful planning of the radiating array. First, the size of the array needs to be estimated based on the target intensity and available input power. This initial design consideration ensures efficient use of the available energy. Next, the spacing between elements within the array must be carefully calculated to eliminate unwanted interference patterns known as grating lobes. These lobes can significantly reduce the intensity at the target point, so their elimination is crucial. Finally, a realizable lens is designed, as discussed above, to achieve the required phase distribution for each radiating element. Since lens design relies on principles of optics, the dimensions for the lens, (G, f) are typically no smaller than four to five wavelengths.

IV. PATH LENGTH ERROR AND RADIATION PATTERNS OF FEED ELEMENTS AT NON-FOCAL POSITIONS ON THE FEED ARRAY CURVE

Since the path length from each of the lens focal points to the corresponding focusing points in the near field is equal for all radiating array elements, the phases are identical at these points. This means that maximum possible power is achieved at B_1, B_2, and B_0 for feed antenna elements at F_2, F_0, and F_1, respectively. In practice, we may need to focus the field at other points in the near field, which requires placing feed antennas at non-focal positions on the feed array curve.

Any antenna placed at a non-focal point will concentrate the field at specific points but, due to phase errors caused by path length discrepancies, there will be some degradation in the focused field, resulting in lower gain, a wider beam, and higher sidelobes. By carefully selecting the parameters of the Rotman lens, these phase errors can be minimized.

The path length error for a point on the feed array curve can be calculated for each radiating array element relative to the center radiating array element using the following formula:

$$Path\ length\ error\,(\Delta L) = \left(\vec{HP}\right) + w + \left(\vec{QB}\right) - \left(\vec{HO_1}\right) - w_0 - \left(\vec{O_2B}\right) . \quad (13)$$

Figure 3 illustrates the path length errors for the lens design given in Fig. 2 (g=1.25) for various values of α, including 0°, 5°, 10°, 15°, 20°, and 25°, where α represents the angle subtended by points on the feed array curve from O_1. The errors for each feed element were determined at the maximum power point along the line connecting B_1 and B_2.

As evident from Fig. 3, the phase errors for the focal points, as anticipated, are zero for all radiating elements. Conversely, path length errors increase as the distance of the feed element from the focal points increases, reaching a maximum path length error of 0.0512 for the feed element located at α=15°. The phase errors can be minimized by selecting the appropriate parameters for a Rotman lens based on the specific design requirements.

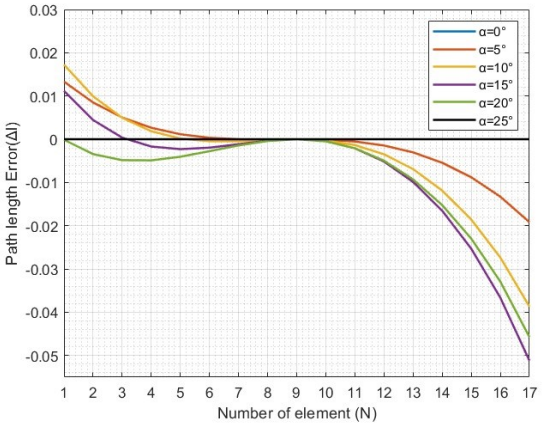

Fig. 3. Path length errors along the radiating array for six points on the feed array curve.

An optical method was employed first to determine the patterns along the line connecting B1 and B2 for the lens design (g=1.25) in Fig. 2. Figure 4 presents these results for various feed port angles (α): 0° (port6), 5° (port7), and so on, up to 25° (port11). Notably, isotropic radiating elements were assumed for this analysis. Due to parameter selection minimizing phase errors, the patterns exhibit minimal degradation.

Next, the design was implemented as a microstrip circuit and simulated using the commercial software CST. Figure 5 depicts the CST implementation of the lens. The design parameters are detailed in Table 2. The radiation patterns of the microstrip lens were then obtained using CST, with the results presented in Fig. 6.

A comparison of Figs. 4 and 6 reveals a high degree of similarity between the radiation patterns obtained

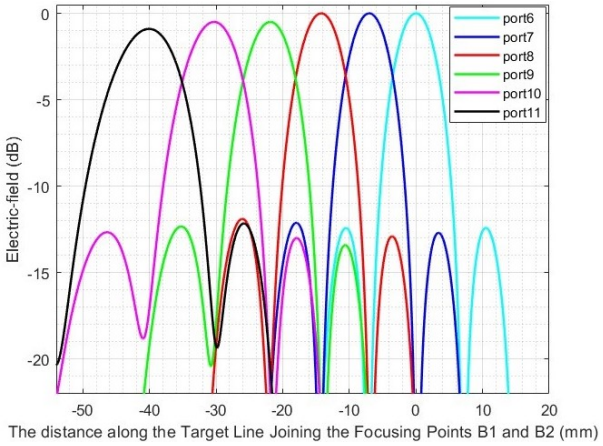

Fig. 4. Radiation patterns for the lens design in Fig. 2 (g=1.25) using optical method.

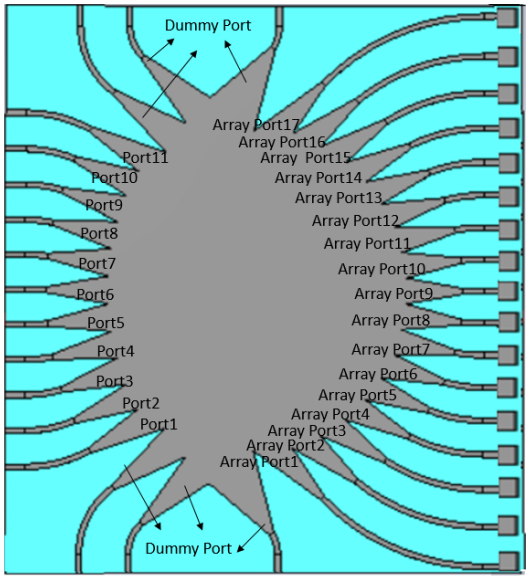

Fig. 5. CST implementation of the lens design.

Table 2: Parameters of the CST lens design

Central frequency	27.5 GHz
ε_r	6.15
Substrate thickness	1.5 mm
Length of feed port and array port tapered lines	18.8 mm
Radiating elements	8 mm × 8 mm
G	60.58 mm
F	48 mm
q	57.70 mm

through the optical and CST methods. However, a key difference exists: the peak electric field strength of the

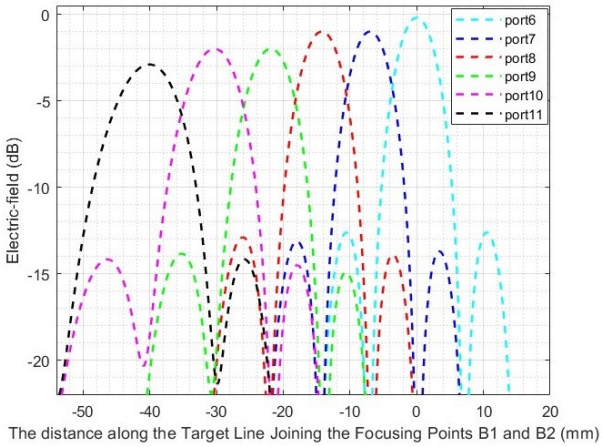

Fig. 6. Radiation patterns for the lens design in Fig. 2 (g=1.25) using CST method.

outer feed elements is lower in the CST implementation. This discrepancy arises because the optical analysis assumed isotropic elements for both the feed array and inner lens elements, while the actual CST implementation utilizes aperture elements with directional patterns.

V. COMPARISON OF NEAR-FIELD PERFORMANCES OF ROTMAN LENSES DESIGNED FOR NEAR FIELD AND FAR FIELD

As has already been stated, achieving the highest field intensity is essential when using electromagnetic fields in the near field for a given input power, therefore a study was conducted to compare the field intensities of two Rotman lens antenna types in the near field. For this comparison, the design of Fig. 2 (g=1.25) was utilized for the near-field-focusing Rotman lens. The far-field-focusing Rotman lens, while maintaining the same parameters, is focused at angles of -35°, 0°, and +35°, corresponding to the angles subtended by the near-field-focusing points B_2, B_0, and B_1.

To calculate total field intensity at a target point, we first determine the phase distribution of each radiating element using lens calculations. Then, we account for the varying distances between the elements and the target point by incorporating a $1/r$ factor when summing the individual field intensities. Although the design of the far-field-focusing lens was carried out for far-field focal points, for fair comparison the field intensity of this lens is also calculated at the same near-field target points.

Figure 7 depicts the electric field intensity for both lenses under identical input power conditions. The fields are positioned along the line joining B_1 and B_2 at the peak points of the near-field-focused Rotman lens, with α values ranging from 0° to 25°. It is clear that the power density of the near-field-focusing lens is 3.8 to 6.3 dB

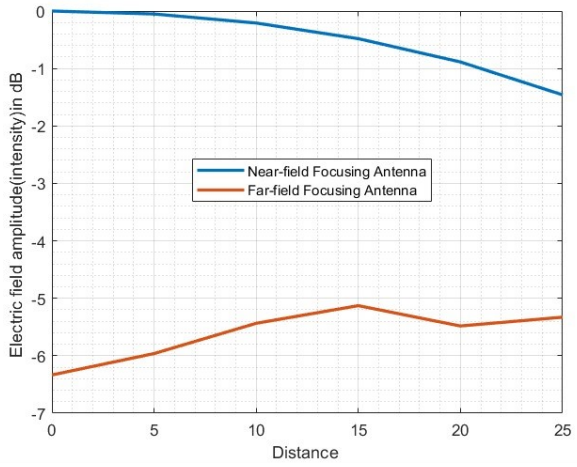

Fig. 7. Maximum electric field intensity along X=q for different positions of feed angle.

higher. These results indicate that the near-field-focusing Rotman lens offers a substantial advantage over the far-field-focusing lens in the near field.

VI. CONCLUSION

Rotman lenses have been demonstrated to be effective multiple beamforming antennas for near-field applications. The design equations for these lenses have been derived, and the inner lens curves and transmission line path lengths have been determined for sample design parameters. These results provide a foundation for the practical realization of Rotman lenses with desired performance characteristics.

The study has shown that by selecting the lens parameters appropriately, the phase errors can be minimized for non-focal points, resulting in only minimal beam deterioration. This is a significant advantage for near-field applications, as it ensures that the Rotman lens can achieve the desired beamforming performance even when the target is not located at the focal point.

A comparison of the power density in the near field has been made for far-field- and near-field-focusing Rotman lenses having the same lens parameters. The results indicate that the power densities of the near-field-focused lens are 3.8 to 6.3 dB higher. This is a significant improvement and makes the near-field-focusing Rotman lens a promising candidate for a wide range of near-field applications.

REFERENCES

[1] P. Nepa and A. Buffi, "Near-field-focused microwave antennas; near-field shaping and implementation," *IEEE Antenna and Propagation Magazine*, vol. 59, no. 3, pp. 42-53, 2017.

[2] A. Buffi, P. Nepa, and G. Manara, "Design criteria for near-field-focused planar arrays," *IEEE Antennas Propag. Mag.,* vol. 54, no. 1, pp. 40–50, Feb. 2012.

[3] S. M. Mikki and Y. M. M. Antar, "A theory of antenna electromagnetic near field-Part I," *IEEE Transactions on Antennas and Propagation*, vol. 59, no. 12, pp. 4691-4705, 2011.

[4] S. M. Mikki and Y. M. M. Antar, "A theory of antenna electromagnetic near field-Part II," *IEEE Transactions on Antennas and Propagation*, vol. 59, no. 12, pp. 4706-4724, 2011.

[5] J. T. Loane III and S.-W. Lee, "Gain optimization of a near-field focusing array for hyperthermia applications," *IEEE Trans. on Microwave Theory and Techniques*, vol. 37, no. 10, pp. 1629–1635, Oct. 1989.

[6] F. Tofigh, J. Nourinia, M. Azarmanesh, and K. M. Khazaei, "Near-field focused array microstrip planar antenna for medical applications," *IEEE Antennas and Wireless Propagation Letters*, vol. 13, pp. 951-954, 2014.

[7] H. Chen, Z. Zhang, and J. Yu, "Near-field scattering of typical targets illuminated by vortex electromagnetic waves," *The Applied Computational Electromagnetics Society Journal (ACES),* vol. 35, no. 2, pp. 129-134, Feb. 2023.

[8] H. Chen, Z. Zhang, and J. Yu, "Resolution of near-field beamforming and its impact on NOMA," *IEEE Wireless Commun. Lett.*, vol. 13, no. 2, pp. 456-460, Feb. 2024.

[9] F. Paredes, C. Herrojo, R. Escudé, E. Ramon, and F. Martin, "High data density near-field chipless-RFID tags with synchronous reading," *IEEE Journal of Radio Freq. Ident.*, vol. 4, no. 4, pp. 517-524, Dec. 2020.

[10] S. H. Zainud-Deen, H. A. Malhat, and K. H. Awadalla, "Dielectric resonator antenna phased array for fixed RFID reader in near field region," in *Japan-Egypt Conference on Electronics, Communications and Computers,* Alexandria, Egypt, pp. 102-107, 2012.

[11] A. Buffi, A. A. Serra, P. Nepa, H. T. Chou, and G. Manara, "A focused planar microstrip array for 2.4 GHz RFID readers," *IEEE Transactions on Antennas and Propagation*, vol. 58, no. 5, pp. 1536-1544, 2010.

[12] Y. Wang, L. Shen, C. Huang, J. Zhu, and W. Tang, "Series-fed dipole array for near-field RFID application," *The Applied Computational Electromagnetics Society Journal (ACES),* vol. 33, no. 11, pp. 1190-1195, Nov. 2018.

[13] M. Bogosanovic and A. G. Williamson, "Microstrip antenna array with a beam focused in the near-field zone for application in non-contact microwave industrial inspection," *IEEE*

Transactions on Instrumentation and Measurement, vol. 56, no. 6, pp. 2186-2195, 2007.

[14] S. Singh and S. P. Singh, "Microstrip slot antenna for hyperthermia applications," in *Applied Electromagnetic Conference (AEMC 2015)*, Guwahati, India, 18-21 Dec. 2015.

[15] W. C. Choi, K. J. Kim, J. Kim, and Y. J. Yoon, "Compact microwave radiator for improving heating uniformity in hyperthermia system," *IEEE Antennas Wireless Propag. Lett.,* vol. 13, pp. 1345-1348, 2014.

[16] W. C. Choi, S. Lim, and Y. J. Yoon, "Design of noninvasive hyperthermia system using transmit-array lens antenna configuration," *IEEE Antennas and Wireless Propagation Letters,* vol. 15, pp. 857-860, 2016.

[17] P. Nayeri, F. Yang, and A. Z. Elsherbeni, "Beam-scanning reflectarray antennas: An overview," in *USNC-URSI National Radio Science Meeting*, Chicago, IL, July 2012.

[18] L. Stark, "Microwave theory of phased-array antennas: a review," *Proc. the IEEE*, pp. 1661-1701, 1974.

[19] W. Rotman and R. F. Turner, "Wide-angle microwave lens for line source applications," *IEEE Trans. Antennas Propag.,* vol. AP-11, no. 6, pp. 623-632, Nov. 1963.

[20] M. J. Maybell, K. K. Chan, and P. S. Simon, "Rotman lens recent developments 1994–2005," in *Proceedings of the 2005 IEEE Antennas and Propagation Society International Symposium*, Washington, DC, 3-8 July 2005.

[21] D. H. Archer and M. J. Maybell, "Rotman lens development history at Raytheon Electronic Warfare Systems 1967-1995," in *Proceeding of the IEEE Antennas and Propagation Society International Symposium,* Washington, DC, pp. 31-34, 2005.

[22] M. Sohail, R. Uyguroğlu, and A.Y. Öztoprak, "Scanning of the near-field focused beam by changing frequency," *The Applied Computational Electromagnetics Society Journal (ACES),* vol. 38, no. 3, pp. 177-183, Mar. 2023.

[23] P. Li, P. Li, P. Yang, Z. Kuang, and X. Luo, "Design of compact Rotman lens with wide-angle scanning using high permittivity substrate," in *2021 International Applied Computational Electromagnetics Society (ACES-China) Symposium*, Chengdu, China, 28-31 July 2021.

[24] T. K. Vo Dai, T. Nguyen, and O. Kilic, "A non-focal Rotman lens design to support cylindrically conformal array antenna," *The Applied Computational Electromagnetics Society Journal (ACES),* vol. 33, no. 2, pp. 240-243, Feb. 2018.

[25] R. Uyguroğlu, A. Y. Öztoprak, and C. Ergün, "Improved phase performance for Rotman lens," *International Journal of RF and Microwave Computer-Aided Engineering,* vol. 23, no. 6, pp. 634-638, Oct. 2013.

[26] H.-T. Chou and D. Torrungrueng, "Development of 2-D generalized tri focal Rotman lens beam-forming network to excite conformal phased arrays of antennas for general near/far-field multi-beam radiations," *IEEE Access,* vol. 9, pp. 49176–49188, 2021.

[27] A.K. Vallappil, M. K. A. Rahim, B. A. Khawaja, N. A. Murad, M. M. Gajibo, "Butler matrix based beamforming networks for phased array antenna systems: A comprehensive review and future directions for 5G applications," *IEEE Access*, vol. 9, pp. 3970-3987, 2021.

[28] R. Uyguroğlu and A. Y. Niazi, "Designing microstrip transitions into parallel plate regions using the FDTD method," *Microwave and Optical Technology Letters*, vol. 22, pp. 81-84, 1999.

Salem M. Otman received his bachelor's degree in Electrical and Electronic Engineering from Bright Star University, Albrega Libya, in 2003, and his master's degree from Cyprus International University in 2018 in the same field. He is currently a Ph.D. student in the Department of Electrical and Electronic Engineering at Cyprus International University. His current research interests include planar antennas, arrays, and near-field-focusing of planar arrays.

Mehmet Kuşaf was born in Larnaca, Cyprus, in December 1973. He received the Ph.D. degree in Electrical and Electronic Engineering from Eastern Mediterranean University in 2005. From 2005 to 2006, he worked as Assistant Professor with the Department of Electrical and Electronics Engineering, European University of Lefke. His academic journey at Cyprus International University began in 2006 as an Assistant Professor, followed by his promotion to Associate Professor in 2009, and culminated as Professor position in 2019. He is currently serving as the Head of Electrical and Electronic Engineering Department. He is the author of many research articles published in esteemed journals. His research expertise includes computational electrodynamics, antennas, and power systems.

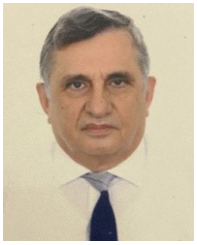

Abdullah Y. Öztoprak earned his Ph.D. in Electrical and Electronic Engineering from University College London, University of London, UK, in 1977. He joined Eastern Mediterranean University (EMU) as an Assistant Professor in 1986, became an Associate Professor in 1988, and progressed to Professor in 1997. During his tenure at EMU, he held various leadership positions, including Chairman of the Department of Electrical and Electronic Engineering (1989-1992), Vice-Rector for Academic Affairs (1992-2003), and Rector (2009-2014). Professor Oztoprak's research focuses on beam forming networks, Rotman lenses, microwave antennas, split-step finite-difference time-domain methods, and unconditionally stable finite-difference time-domain methods.